P2X7R promotes angiogenesis and tumor-associated macrophage recruitment by regulating the NF-κB signaling pathway in colorectal cancer cells

Chunhui Yang
Dalian Medical University
shuang shi
Dalian Medical University
Ying Su
Dalian Medical University
jingshan tong (tongjingshan@gmail.com)
UPMC Hillman Cancer Center
Liangjun Li
Dalian Medical University

Research

Keywords:

Posted Date: May 11th, 2020

DOI: https://doi.org/10.21203/rs.3.rs-27043/v1

Abstract

Background

Overexpression of P2 × 7R has been observed in several tumors and is related to cancer advancement and metastasis. However, the role of P2 × 7R in colorectal cancer (CRC) patients is not well understood.

Methods

In the current study, overexpression of P2 × 7R and the effects at the molecular and functional levels in CRC were assessed in a mouse orthotopic model. Functional assays, such as the CCK-8 assay, wound healing and transwell assay, were used to determine the biological role of P2 × 7R in CRC cells. CSC-related genes and properties were detected via sphere formation and real-time PCR assays. The underlying mechanisms were explored by Western blotting, real-time PCR and Flow cytometry.

Results

In this study, we found that overexpression of P2 × 7R increase in the *in vivo* growth of tumors. P2 × 7R overexpression also increased CD31, VEGF and concurrent angiogenesis. P2 × 7R upregulates aldehyde dehydrogenase-1 (ALDH1) and CSC characteristics. Transplanted tumor cells with P2 × 7R overexpression stimulated cytokines to recruit TAMs to increase the growth of tumors. We also found that the NF-κB signaling pathway is involved in P2 × 7R-induced cytokine upregulation.

Conclusion

P2 × 7R promotes NF-κB-dependent cytokine induction, which leads to tumor-associated macrophage (TAM) recruitment to control tumor growth and advancement and remodeling of the stroma. Our findings demonstrate that P2 × 7R plays a key role in TAM recruitment, which may be a therapeutic target for CRC patients.

Background

The number of deaths due to colorectal cancer (CRC) stands at 0.7 million with diagnosis of 1.4 million new cases across the globe(1, 2). The heterogeneous nature of this disease suggests the involvement of genetics such as chromosomal and microsatellite instability and epigenetics such as the CpG island methylation phenotypes(3–5).

Angiogenesis and the ability to metastasize involve tumor-associated macrophages (TAMs) in CRC(6, 7). M1 and M2 are the major classes of TAMs that display polar effects on tumors(8, 9). The former class is activated classically by lipopolysaccharide (LPS) and interferon-γ (IFN-γ) to secrete interleukin-12 (IL-12),

IL-1β and cytotoxic inducible nitric oxide synthase (iNOS), among other factors(10, 11). Alternative activation is observed in M2 macrophages due to IL-4, IL-10 or IL-13, which express vascular endothelial growth factor (VEGF) and other factors for angiogenesis, as well as IL-6 and IL-10(12, 13). The infiltration of increased numbers of M2 macrophages is associated with poor prognosis in patients with colon cancer(6, 14). TAM polarization and differentiation is controlled by the microenvironment and tumor cells themselves by means of cytokines synthesized by the latter(15, 16).

Lymphocytes express P2 × 7R (P2X purinoceptor 7) to control activation of T cells (mainly T helper 1 (Th1) and Th17 cells) via extracellular adenosine 5'-triphosphate (ATP) secreted by damaged cells(17, 18). These T cells function in alloimmune responses as well as the rejection of allografts(19). The receptor, which exists in several single nucleotide polymorphisms (SNPs) and splice isoforms (A–J) correlate with many diseases. The P2 × 7R is a ligand-gated ion channel permeable to Ca^{2+}, K^{+} and Na^{+} (20). Prolonged stimulation of this receptor leads to pore formation that causes the entry of large molecules, resulting in cell lysis and mortality(21). Several of the functions of P2 × 7R in cancer include inducing cell death and serving as an antitumor receptor(21, 22). Another role involves in sustaining the and the ability of cancer cells to migrate and invade *in vitro* and *in vivo*(23). These apparently contradictory roles can be explained by the involvement of isoforms: P2 × 7A for apoptosis and P2 × 7B for stimulation(24). Because the involvement of P2 × 7R in modulating the immune system and inflammatory pathways is known, its role in tumor biology is of interest, especially because this receptor is overexpressed in several tumors and is linked to reduced survival and increased advancement and metastasis.

This work is an investigation of the involvement of P2 × 7R in the function of CRC cells. The observations show an increase in cancer stem cells (CSCs), VEGF upregulation to cause angiogenesis and increased growth of tumors *in vivo*. Overexpression of P2 × 7R caused TAM recruitment via the involvement of high levels of VEGF, (C-C motif) ligand 2/5 (CCL2/5) and macrophage-specific colony stimulating factor (CSF-1).

Materials And Methods

Cell culture

Human CRC cell lines, including HCT116, DLD1, SW837, and RKO and the BALB/C-derived mouse colon adenocarcinoma cell line CT26, were obtained from ATCC (American Type Culture Collection, USA). All cell lines were cultured in Dulbecco's modified Eagle's medium (DMEM) with 4.5 g/L glucose (Mediatech) supplemented with 10% FBS at 37℃ in a humidified atmosphere of 5% CO_2.

P2X7R overexpression and knockdown

Generation of pcDNA3.1-hP2X7R, an expression plasmid for P2X7R, was performed as previously described(25). Lipofectamine 3000 was used to transfect RKO and HCT116 cells using the control pcDNA3.1 or pcDNA3.1-hP2X7R. pcDNA3.1-mP2X7R was constructed by cloning murine P2X7R cDNA

into the EcoRI and NotI sites of pcDNA3.1. This was followed by the stable transfection of CT26 cells using control pcDNA3.1 or pcDNA3.1-mP2X7R and Lipofectamine 3000 (Invitrogen) according to the prescribed protocols. Zeocin (300 μg/mL, Invitrogen) in the medium of CT26-Con and CT26-mP2X7R cells was used to select stable transfectants.

Lipofectamine 3000 was utilized for transfection of HEK293T cells with green fluorescent protein (GFP)-tagged lentiviral (pGIPZ) constructs containing P2X7R shRNA (sh*P2X7R*) or scrambled shRNA (shCon; Dharmacon) and pCMV-Δ8.2 and pCMV-VSVG packaging plasmids (Addgene). At 72 hours after transfection, viral supernatants were collected, followed by instant infection in the presence of 10 μg/mL polybrene (Sigma-Aldrich). Puromycin at a concentration of 5 μg/mL was utilized for the selection of the abovementioned transfectants, which were subjected to cell sorting, and the top 10-20% cells with staining for GFP were collected.

Animal models

The Second Affiliated Hospital of Dalian Medical University Institutional Animal Care and Use Committee guidelines issued approval for the experiments. The establishment of the orthotopic CRC mouse model was in accordance with a previously described protocol(26). Briefly, 2% isoflurane in oxygen was administered to BALB/C mice (8 weeks of age) by inhalation for anesthesia. The cecum was exposed by making a midline incision. A 33-gauge microinjector (Hamilton) was used to inject 10 μL of 2×10^6 CT26-Con or CT26-mP2X7R cells in phosphate buffered saline (PBS) into the subserosa of the cecum. Tissue adhesive (3M) was used to seal the site to avoid leakage, followed by washing with 70% alcohol and PBS. Then, 6-0 polyglycolic acid sutures (CP Medical) were used for skin and abdominal wall closure following the replacement of the cecum in the peritoneal cavity. The sacrifice of the animals was performed 6 weeks after the cell implantation, followed by measuring the tumor weights and processing the tumors.

Histology and immunohistochemistry

The processing of tumor samples was performed in accordance with previously established protocols(27, 28). Normal horse serum (Jackson ImmunoResearch) was applied for 60 min to block nonspecific epitopes. This was followed by incubation of the sections at 4°C overnight with primary antibodies. For immunohistochemistry, the 2-Solution diaminobenzidine (DAB) kit (Invitrogen) was utilized to detect signals following a 60 min incubation with suitable secondary antibodies conjugated to HRP (Bio-Rad, Hercules) at room temperature. This was followed by hematoxylin counterstaining and mounting in Acrymount (StatLab).

Cell growth assay

A total of 3000 human CRC cells in 100 μL of complete culture media per well were added to 96-well plates. CCK-8 (Sigma-Aldrich) reagent was utilized to assess proliferation at 72 hours after plating in accordance with the manufacturer's protocols.

Western blotting

Western blotting was performed as previously described(26). Briefly, RIPA buffer (Pierce, Rockford, IL) was utilized to prepare whole cell lysates as previously described. Centrifugation of the final lysate was performed at 13,000 g for 15 min at 4℃. Reduction of the samples was performed by heating for 10 min with 50 mM DTT at 98℃. Ten percent polyacrylamide precast gels (Invitrogen) were used to separate 50 µg of protein, followed by blotting to PVDF membranes (Invitrogen). This was followed by blocking the membranes with a 5% skim milk solution in TBS-Tween 0.05% buffer at room temperature for 60 min. Next, the membranes were incubated overnight with primary antibodies at 4℃. Secondary antibodies conjugated to HRP were incubated with the blots, followed by development using EZ-ECL (Biological Industries) and visualization on a Fusion FX (Vilber Lourmat).

Flow cytometry analysis

Anti-CD44 conjugated to FITC and anti-CD166 conjugated to PE were used for staining CT26-Con and CT26-mP2X7R cells. Sequential enzymatic digestion was utilized to obtain single-cell suspensions from tumors as previously described(29). A 70 µm nylon cell strainer (BD Biosciences) was utilized to filter the suspensions, followed by double PBS washing. Staining of the isolated CT26-Con or CT26-mP2X7R cells was performed using anti-Gr1-FITC, CD11b-APC and anti-F4/80-PE (eBioscience; San Diego). A total of 1×10^6 cells was incubated with antibodies in 100 µL wash buffer (PBS plus 0.1% BSA) for 60 min at 4°C. After washing with the same cold buffer, 1% paraformaldehyde was utilized for fixation. A BD LSRII flow cytometer (BD Biosciences) was utilized for flow cytometric analysis of 30 000 cells.

In vitro formation of tumorspheres

Ultralow attachment 6-well plates (Corning) were used to plate CT26-Con, CT26-mP2X7R, HCT116-Con, HCT116-hP2X7R, HCT116-sh con and HCT116-sh hP2X7R cells (10000 per well) in 2 mL of serum-free medium in accordance with previously established protocols. After one week of culture at 37°C and 5% CO_2, manual counting of the tumorspheres was performed for each well.

Assessing wound healing, migratory and invasive abilities

CT26-Con and CT26-mP2X7R cells were seeded in six-well plates and cultured until reaching 90% confluence. A sterile 200 µL pipette tip was utilized to wound the monolayers, followed by incubation in DMEM plus 1% FBS for 24 or 48 hours under standard conditions. Marking and photography of the wounded areas before and after incubation was performed. ImageJ (NIH) was utilized to measure the area of the wound to assess the repair in triplicate assays and triplicate wells. The ability of the P2X7R-overexpressing cells and appropriate controls and P2X7R-knockdown cells and their appropriate controls to invade and migrate was performed in accordance with a previous protocol in triplicate across triplicate wells.

Real-time PCR

Real-time PCR was performed as previously described(30). Briefly, a Total RNA Isolation Mini Kit (Agilent) was utilized to isolate the total RNA from cells. The RevertAid First Strand cDNA synthesis kit (Fermentas) was used to synthesize complementary DNA. The RT-PCR cDNA involved the use of primers, Jumpstart Taq DNA and a dNTP mix. The parameters included one cycle for 1 min at 95℃, 45 cycles for 20 s at 95℃, 30 s at 57℃, and 1 min at 72℃, and one final cycle for 5 min at 72℃. Roche FastStart Universal SYBR Green Master (ROX) was utilized for the real-time PCRs using the following parameters: one cycle for 2 min at 50℃ and one cycle for 10 min at 95℃. Subsequently, 35 amplification cycles of 15 s at 95℃, 60 s at 57℃, and 60 s at 72℃ were performed. The final step was a dissociation step for 15 s at 95℃ and 15 s each at 60℃ and 95℃.

Statistical analysis

The data are expressed as the mean ± standard deviation (SD). The comparison of 2 sets was performed utilizing Student's *t*-test, while one-way ANOVA followed by Dunnett's test was utilized for more than 2 data samples. Significance was considered at $P < 0.05$, $P < 0.01$ or $P < 0.001$, which are represented by *, ** or ***, respectively.

Results

P2X7R promotes CRC cell proliferation, migration and invasion *in vitro*

To investigate the role of P2X7R in CRC cells, we assessed the *in vitro* effect of P2X7R overexpression on CT26 cells. Our results indicated that P2X7R promoted the proliferation of CT26 cells (**Figure 1A**). This was followed by studying the changes in behavior due to P2X7R overexpression. CT26-mP2X7R cells migrated at a higher rate compared to that of CT26-Con cells, as observed in the wound healing assay (**Figure 1B**). CT26-mP2X7R cells showed an increased ability to invade compared to that of CT26-Con cells (**Figure 1C**). This trend was also displayed by HCT116 and RKO cells in terms of invasion (**Figure S1A and S1B**) and migration ability (**Figure S1C and S1D**). In contrast, P2X7R knockdown reduced the abilities of CT26 and DLD1 cells to migrate and invade (**Figure 1D and S1E-S1F**). These observations indicate that the increased abilities of CRC lines to migrate and invade *in vitro* were due to P2X7R.

A crucial step in tumorigenesis is the epithelial-mesenchymal transition (EMT), which boosts the ability of epithelial cells to migrate and invade, facilitating metastasis(31, 32). The involvement of P2X7R in this phenomenon has been documented in many cancers(33). This work examined the levels of proteins involved in the EMT by western blot analysis of CT26-mP2X7R and CT26-Con cells. There was a marginal reduction in E-cadherin and induction of N-cadherin and Vimentin (**Figure 1F**). shRNA-mediated blocking of P2X7R resulted in an evident increase in E-cadherin in CT26 and DLD1 cells (**Figure S1G-S1H**). Overall, these observations indicate a lack of likely and vital involvement of the EMT in the response in the cell lines studied to P2X7R overexpression.

P2X7R enhances the growth of CRC tumors *in vivo*

The involvement of P2X7R overexpression in the advancement of CRC was assessed using a surgical orthotopic mouse model. The formation of primary tumors was observed in 8 of the 10 mice, with an average tumor weight of ~360 mg (**Figure 2A-2B**). This was a stark difference from the tumors formed in 3 of the 10 mice administered CT26-Con cells, with an average tumor weight of ~110 mg. This shows a conspicuous increase in the growth and weight of tumors due to P2X7R overexpression.

The CT26-Con or CT26-mP2X7R tumors that formed in the cecum were assessed for their properties to explore the role of P2X7R in CRC. Immunohistochemistry was performed for Ki67, a proliferation marker, and cleaved caspase-3, an apoptosis marker, because the abovementioned tumor increases may be due to increased proliferation or reduced apoptosis. The number of cells that were positive for Ki67 was higher in CT26-mP2X7R cells compared to that of CT26-Con cells, while the expression of cleaved caspase-3 was lower in CT26-mP2X7R than CT26-Con cells (**Figure 2C and 2D**), which suggests that P2X7R induces increased proliferation of cells in tumors, as well as reduced apoptosis rates.

P2X7R promotes CRC tumor angiogenesis

Tumors expressing high levels of P2X7R and controls displayed the phenotype of a hypercellular solid carcinoma with high mitosis and high-grade atypia. The occurrence of vascular endothelial cells and pericytes was examined by staining for CD31 and α-SMA, respectively, in the formed vessels. The staining was more pronounced in the CT26-mP2X7R tumors compared with that of CT26-Con tumors (**Figure 3A**), indicating increased angiogenesis in the tumors due to P2X7R overexpression. This was followed by examining the protein expression of angiogenic and metastatic proteins in the serum of the mice. The protein levels of VEGF, MMP9, MMP2 and LOX increased in the sera of CT26-P2X7R tumor-bearing mice compared with those of CT26-Con mice (**Figure 3B**). The MMP9, VEGF and LOX levels were higher in CT26-mP2X7R mice compared to those of CT26-Con mice, as shown by immunohistochemistry (**Figure 3C**), which indicates an increase in expression in the serum rather than increased sizes of CT26-P2X7R compared to that of CT26-Con mice. Additionally, the *in vitro* protein levels of MMP9, VEGF, and MMP2 were higher in CT26-mP2X7R cells relative to those of CT26-Con cells (**Figure 3D**). This suggests that angiogenesis was stimulated by P2X7R overexpression via the abovementioned factors in CRC.

P2X7R increases the features of CSCs in CRC

Next, we examined the potential development of CSC features in CRC by P2X7R by examining ALDH1 levels in the tumors and in culture. The ALDH1 levels were considerably higher in the tumors and cultures of CT26-mP2X7R cells compared to those of CT26-Con cells (**Figure 4A and 4B**). The expression of CD44+ and CD166+ was examined by flow cytometry because these antigens are markers of CSC. There was a conspicuous increase in the number of cells expressing these markers in CT26-mP2X7R cells compared to that of CT26-Con cells (**Figure 4C**). Tumorsphere formation ability was assessed next. CT26-mP2X7R cells displayed more tumorspheres compared to that of CT26-Con cells (**Figure 4D**). A similar study was conducted on human CRC cells with knockdown or overexpression of P2X7R. Overexpression of P2X7R was performed in HCT116 cells because the levels of the receptor are low in this cell line. P2X7R overexpression increased the number of tumorspheres in HCT116 cells (**Figure 4E**). However,

P2X7R knockdown decreased tumorsphere numbers in HCT116 cells (**Figure 4F**). Hence, the number of cells displaying CSC properties was increased by P2X7R overexpression.

P2X7R boosts TAM recruitment in CT26 tumors

The infiltration of various types of immune cells, such as TAMs, neutrophils, natural killer (NK) cells and T cells, has been observed in CRC(34, 35). Flow cytometry was performed to examined the types of infiltrating cells coupled with immunostaining that showed minor alterations in T cells, NK cells, mast cells and B cells (data not shown). CT26-mP2X7R tumors showed an evident increase in cells expressing macrophage markers (F4/80 and CD11b) compared to that of CT26-Con tumors, which indicates a boost in infiltration of macrophages due to P2X7R overexpression (**Figure 5A**). The cell population expressing neutrophil markers (CD11b+ and Gr1+) was reduced in few CT26-mP2X7R tumors compared with that of the controls but was not significant (**Figure 5B**). Immunohistochemistry showed that macrophages that were positive for F4/80 formed clusters in CT26-mP2X7R tumors compared to that of the control CT26-Con tumors (**Figure 5C**). These indicate that P2X7R overexpression results in TAM recruitment and stimulation of angiogenesis in the tumors. This increase in macrophages is likely due to tumor cell recruitment and not systemic inflammation.

P2X7R augments TAM recruitment by increasing cytokines

The tumors did not display cytotoxicity and were boosted by TAMs via the synthesis of growth factors, chemokines and cytokines, resulting in angiogenesis and remodeling of tissues(36). The recruitment of TAMs to CRC tumors involves CCL2, CCL5, VEGF and CSF-1(37, 38). The mRNA levels of these molecules were higher in CT26-mP2X7R cells compared to those of CT26-Con cells (**Figure 6A**). The mRNA expression of cytokines involved in neutrophil recruitment to cancer sites, such as colony stimulating factor-2 (CSF-2), CSF-3 and chemokine (C-X-C motif) ligand 1 (CXCL1) were determined, and CSF-2 and CSF-3 were reduced and CXCL1 expression was increased in CT26-mP2X7R cells (**Figure 6B**). The mRNA levels of HIF-1α and HIF-1β were assessed in CT26-Con and CT26-mP2X7R cells because TAM recruitment was observed in tumors and hypoxic sites. The mRNA levels of both of these genes were increased in CT26-P2X7R cells (**Figure 6C**). Expression of cytokines associated with macrophage recruitment was also assessed in human cell lines. The mRNA (**Figure 6D**) and protein (**Figure 6F**) levels of CCL2, CSF-1 and CCL5 were higher in HCT116 and RKO cells overexpressing P2X7R compared with those of the controls. Thus, these data suggest an increase in cytokines that are involved in the infiltration of macrophages in tumors, which manifests as tumorigenesis.

Augmented and prolonged NF-κB signaling by P2X7R

The mechanism of P2X7R in tumorigenesis was assessed by studying many pathways involved in cancer using luciferase reporter assays. The pathways studied included NF-κB (nuclear factor-κB), p53, Wnt/β-catenin (TOP flash/FOP flash), TGF-β, p21, STAT3 (APRE), p38, and STAT5 (LHRE) (data not shown). The expression of ectopic P2X7R distinctly increased the reporter expression of NF-κB luciferase in CT26 and HCT116 cells (**Figure 7A**). This signaling was inhibited by P2X7R knockdown in DLD1 and

SW837 cells (**Figure 7B**). Next, CAPE and JSH-23, specific inhibitors of NF-κB, were used to treat cells that expressed or lacked expression of ectopic P2X7R. The proliferation of CT26 cells was markedly lowered by treatment with the inhibitors, which suggests that the NF-κB pathway is activated in CRC tumorigenesis by P2X7R (**Figure 7C**). Furthermore, CAPE treatment or p65 knockdown blocked P2X7R overexpression-induced CSF-1 and CCL2/5 induction **(Figure 7D-7E)**. The above data indicate that the NF-κB signaling pathway mediates P2X7R-induced generation of CSF-1 and CCL2/5, TAM recruitment, and tumor progression.

Discussion

This study demonstrated reduced survival due to P2 × 7R overexpression in CRC at advanced stages, as well as augmented tumorigenesis, angiogenesis and metastasis in the CT26 CRC cell line *in vivo*. An increase in the CSC properties an altered chemokine profiles that attract macrophages all contribute to the tumorigenesis and spread of CRC. The NF-κB signaling pathway was found to be activated and may play a role in the function of P2 × 7R in CRC cells.

Expression of the P2 × 7 receptor is higher in tumors than in normal samples at both the protein and mRNA levels. A vital feature behind the aggressiveness of CRC is the spread of cells due to invasion. P2 × 7R overexpression was found to boost these abilities *in vitro*. These observations are in contrast to the involvement of P2 × 7R in influencing the migration of cancer of the prostate, lungs and breast. The EMT is a vital step in metastasis that is manifested as a deficit in E-cadherin(39). This study reported a conspicuous reduction in E-cadherin in CRC cells and a minor reduction in E-cadherin in CRC cells, which were all cell lines with P2 × 7R overexpression. P2 × 7R knockdown resulted in an increase in E-cadherin in CRC cells. These results suggest the possibility of EMT involvement in the ability of CRC to migrate and invade in certain instances, with the degree of transition dependent on the cell line. P2 × 7R overexpression also increased VEGF and MMP9, which increased blood vessel formation and metastasis, suggesting a mechanism for P2 × 7R in CRC tumorigenesis.

The formation of new blood vessels supports the metabolic needs of tumors as well as allowing for the escape of cells to spread the disease(40). Tumor cells were implanted as described to construct a murine model that showed that the higher levels of P2 × 7R caused changes in the tumor stroma via TAM recruitment and angiogenesis, as well as increased CSC features. The tumor microenvironment is critical in the process of metastasis(41). As previously mentioned, metastasis involves M2 but not M1 macrophages that support tumor formation(42). This stage prior to metastasis involves the several factors, including cytokines and immune cells, such as neutrophils and regulatory/suppressor cells(43). The formation of the premetastatic niche involves the secretion of factors by the tumor to stimulate resident macrophages and recruit macrophages/monocytes(44). However, the involvement of TAMs as safe havens for tumor cells, especially in distant organs, has recently received more widespread research attention. The tumor microenvironment involves crucial stromal cells that undergo recruitment by cancer cells to boost the advancement and metastasis of the latter(45). Angiogenesis is initiated by the secretion of VEGF, a major factor that causes the induction and proliferation of endothelial cells(46).

The involvement of macrophages or TAMs in tumorigenesis is being slowly unraveled(47). In the first stages, a proinflammatory environment is maintained by the macrophages, while in later steps, angiogenesis is favored with an augmentation of the ability of tumor cells to migrate and invade and control antitumor immunity(48). CRC and other cancers, for instance, show high levels of CSF-1, a vital macrophage regulator that is linked to poor prognosis(49). The expression of transcription factors regulating angiogenesis, such as VEGF:HIF-1α, is constitutively observed in macrophages that are located in hypoxic tumor sites(50). MMP9 synthesized by macrophages upon cues from tumor cells allows for invasion by disruption of the extracellular matrix(51). The present work reports infiltration of TAMs by altering the expression of several chemokines in a murine model. These TAMs produce molecules that favor tumor biology, such as MMP9 and VEGF that allow for angiogenesis and metastasis.

Conclusions

In summary, the present work showed that P2 × 7R overexpression promotes cancer aggressiveness and correlates with macrophage infiltration in CRC and provides new insight into the roles of P2 × 7R in immune modulation. These findings point towards the P2 × 7R/NF-κB/CSF-1 and CCL2/5 macrophage axes as potential therapeutic targets in CRC.

Abbreviations

ALDH1: aldehyde dehydrogenase-1; ATCC: American Type Culture Collection; ATP: adenosine 5'-triphosphate; CCL2/5: (C-C motif) ligand 2/5; CRC: colorectal cancer; CSCs: cancer stem cells; CSF-1: colony stimulating factor-1; CXCL1: chemokine (C-X-C motif) ligand 1; DAB: 2-Solution diaminobenzidine; DMEM: Dulbecco's modified Eagle's medium; EMT: epithelial-mesenchymal transition; IFN-γ: interferon-γ; IL-12: interleukin-12; iNOS: inducible nitric oxide synthase; LPS: lipopolysaccharide; PBS: phosphate buffered saline; SNPs: single nucleotide polymorphisms; TAM: tumor-associated macrophage; Th1: T helper 1; VEGF: vascular endothelial growth factor.

Declarations

Ethics approval and consent to participate

This study was approved by the Ethical Committee of the Second Affiliated Hospital of Dalian Medical University.

Consent for publication

Informed consent was obtained from all individual participants included in the study.

Availability of data and materials

All data generated or analyzed during this study are included in this published article.

Competing interests

The authors declare that they have no conflicts of interest.

Funding

No applicable

Author contributions

LL and JST developed the hypothesis, designed the experiments, and revised the manuscript. CY, SS, YS and LL performed the experiments and statistical analyses.

Acknowledgements

No applicable

References

1. Siegel RL, Miller KD, Jemal A. Cancer statistics, 2019. CA Cancer J Clin. 2019;69(1):7–34.
2. Keum N, Giovannucci E. Global burden of colorectal cancer: emerging trends, risk factors and prevention strategies. Nat Rev Gastroenterol Hepatol. 2019;16(12):713–32.
3. Hong SN. Genetic and epigenetic alterations of colorectal cancer. Intest Res. 2018;16(3):327–37.
4. Danese E, et al. Comparison of genetic and epigenetic alterations of primary tumors and matched plasma samples in patients with colorectal cancer. PLoS One. 2015;10(5):e0126417.
5. Migliore L, Migheli F, Spisni R, Coppede F. Genetics, cytogenetics, and epigenetics of colorectal cancer. J Biomed Biotechnol. 2011;2011:792362.
6. Yahaya MAF, Lila MAM, Ismail S, Zainol M, Afizan N. (2019) Tumour-Associated Macrophages (TAMs) in Colon Cancer and How to Reeducate Them. *J Immunol Res* 2019:2368249.
7. Badawi MA, Abouelfadl DM, El-Sharkawy SL, El-Aal WE, Abbas NF. Tumor-Associated Macrophage (TAM) and Angiogenesis in Human Colon Carcinoma. Open Access Maced J Med Sci. 2015;3(2):209–14.
8. Zheng X, et al. Redirecting tumor-associated macrophages to become tumoricidal effectors as a novel strategy for cancer therapy. Oncotarget. 2017;8(29):48436–52.
9. Lee C, et al. Targeting of M2-like tumor-associated macrophages with a melittin-based pro-apoptotic peptide. J Immunother Cancer. 2019;7(1):147.
10. Genard G, Lucas S, Michiels C. Reprogramming of Tumor-Associated Macrophages with Anticancer Therapies: Radiotherapy versus Chemo- and Immunotherapies. Front Immunol. 2017;8:828.
11. Almatroodi SA, McDonald CF, Darby IA, Pouniotis DS. Characterization of M1/M2 Tumour-Associated Macrophages (TAMs) and Th1/Th2 Cytokine Profiles in Patients with NSCLC. Cancer Microenviron. 2016;9(1):1–11.

12. Genin M, Clement F, Fattaccioli A, Raes M, Michiels C. M1 and M2 macrophages derived from THP-1 cells differentially modulate the response of cancer cells to etoposide. BMC Cancer. 2015;15:577.
13. Chen Y, et al. Tumor-associated macrophages: an accomplice in solid tumor progression. J Biomed Sci. 2019;26(1):78.
14. Zhong X, Chen B, Yang Z. The Role of Tumor-Associated Macrophages in Colorectal Carcinoma Progression. Cell Physiol Biochem. 2018;45(1):356–65.
15. Lin Y, Xu J, Lan H. Tumor-associated macrophages in tumor metastasis: biological roles and clinical therapeutic applications. J Hematol Oncol. 2019;12(1):76.
16. Yang L, Zhang Y. Tumor-associated macrophages: from basic research to clinical application. J Hematol Oncol. 2017;10(1):58.
17. Savio LEB, de Andrade Mello P, da Silva CG, Coutinho-Silva R. The P2 × 7 Receptor in Inflammatory Diseases: Angel or Demon? Front Pharmacol. 2018;9:52.
18. Di Virgilio F, Dal Ben D, Sarti AC, Giuliani AL, Falzoni S. The P2 × 7 Receptor in Infection and Inflammation. Immunity. 2017;47(1):15–31.
19. Adinolfi E, et al. The P2 × 7 receptor: A main player in inflammation. Biochem Pharmacol. 2018;151:234–44.
20. Tao JH,, et al. Single nucleotide polymorphisms associated with P2 × 7R function regulate the onset of gouty arthritis. PLoS One. 2017;12(8):e0181685.
21. Burnstock G, Knight GE. The potential of P2 × 7 receptors as a therapeutic target, including inflammation and tumour progression. Purinergic Signal. 2018;14(1):1–18.
22. Park M, et al. Involvement of the P2 × 7 receptor in the migration and metastasis of tamoxifen-resistant breast cancer: effects on small extracellular vesicles production. Sci Rep. 2019;9(1):11587.
23. Ji Z, et al. (2018) Involvement of P2 × 7 Receptor in Proliferation and Migration of Human Glioma Cells. *Biomed Res Int* 2018:8591397.
24. Roger S, et al. Understanding the roles of the P2 × 7 receptor in solid tumour progression and therapeutic perspectives. Biochim Biophys Acta. 2015;1848(10 Pt B):2584–602.
25. Han B, et al. The novel proteasome inhibitor carfilzomib activates and enhances extrinsic apoptosis involving stabilization of death receptor 5. Oncotarget. 2015;6(19):17532–42.
26. Tan X, Zhang Z, Yao H, Shen L. Tim-4 promotes the growth of colorectal cancer by activating angiogenesis and recruiting tumor-associated macrophages via the PI3K/AKT/mTOR signaling pathway. Cancer Lett. 2018;436:119–28.
27. Tan X, et al. BET Inhibitors Potentiate Chemotherapy and Killing of SPOP-Mutant Colon Cancer Cells via Induction of DR5. Cancer Res. 2019;79(6):1191–203.
28. Zhang Z, et al. GNA13 promotes tumor growth and angiogenesis by upregulating CXC chemokines via the NF-kappaB signaling pathway in colorectal cancer cells. Cancer Med. 2018;7(11):5611–20.
29. Bertrand F, et al. TNFalpha blockade overcomes resistance to anti-PD-1 in experimental melanoma. Nat Commun. 2017;8(1):2256.

30. Tong J, et al. Mcl-1 Phosphorylation without Degradation Mediates Sensitivity to HDAC Inhibitors by Liberating BH3-Only Proteins. Cancer Res. 2018;78(16):4704–15.
31. Pearson GW. (2019) Control of Invasion by Epithelial-to-Mesenchymal Transition Programs during Metastasis. *J Clin Med* 8(5).
32. Lu W, Kang Y. Epithelial-Mesenchymal Plasticity in Cancer Progression and Metastasis. Dev Cell. 2019;49(3):361–74.
33. Skovierova H, Okajcekova T, Strnadel J, Vidomanova E, Halasova E. Molecular regulation of epithelial-to-mesenchymal transition in tumorigenesis (Review). Int J Mol Med. 2018;41(3):1187–200.
34. van Dalen FJ, van Stevendaal M, Fennemann FL, Verdoes M, Ilina O. (2018) Molecular Repolarisation of Tumour-Associated Macrophages. *Molecules* 24(1).
35. Carotta S. Targeting NK Cells for Anticancer Immunotherapy: Clinical and Preclinical Approaches. Front Immunol. 2016;7:152.
36. Zhang R, et al. Cancer-associated fibroblasts enhance tumor-associated macrophages enrichment and suppress NK cells function in colorectal cancer. Cell Death Dis. 2019;10(4):273.
37. Dwyer AR, Greenland EL, Pixley FJ. (2017) Promotion of Tumor Invasion by Tumor-Associated Macrophages: The Role of CSF-1-Activated Phosphatidylinositol 3 Kinase and Src Family Kinase Motility Signaling. *Cancers (Basel)* 9(6).
38. Avila MA, Berasain C. Targeting CCL2/CCR2 in Tumor-Infiltrating Macrophages: A Tool Emerging Out of the Box Against Hepatocellular Carcinoma. Cell Mol Gastroenterol Hepatol. 2019;7(2):293–4.
39. Gheldof A, Berx G. Cadherins and epithelial-to-mesenchymal transition. Prog Mol Biol Transl Sci. 2013;116:317–36.
40. Forster JC, Harriss-Phillips WM, Douglass MJ, Bezak E. A review of the development of tumor vasculature and its effects on the tumor microenvironment. Hypoxia (Auckl). 2017;5:21–32.
41. Sleeboom JJF, Eslami Amirabadi H, Nair P, Sahlgren CM, den Toonder JMJ. (2018) Metastasis in context: modeling the tumor microenvironment with cancer-on-a-chip approaches. *Dis Model Mech* 11(3).
42. Poh AR, Ernst M. Targeting Macrophages in Cancer: From Bench to Bedside. Front Oncol. 2018;8:49.
43. Yao M, Brummer G, Acevedo D, Cheng N. Cytokine Regulation of Metastasis and Tumorigenicity. Adv Cancer Res. 2016;132:265–367.
44. Esquivel-Velazquez M, et al. The role of cytokines in breast cancer development and progression. J Interferon Cytokine Res. 2015;35(1):1–16.
45. Joshi S, et al. Rac2 controls tumor growth, metastasis and M1-M2 macrophage differentiation in vivo. PLoS One. 2014;9(4):e95893.
46. Zhao Y, Adjei AA. Targeting Angiogenesis in Cancer Therapy: Moving Beyond Vascular Endothelial Growth Factor. Oncologist. 2015;20(6):660–73.

47. Guo Q, et al. (2016) New Mechanisms of Tumor-Associated Macrophages on Promoting Tumor Progression: Recent Research Advances and Potential Targets for Tumor Immunotherapy. *J Immunol Res* 2016:9720912.
48. Petty AJ, Yang Y. Tumor-associated macrophages: implications in cancer immunotherapy. Immunotherapy. 2017;9(3):289–302.
49. Hoves S, et al. Rapid activation of tumor-associated macrophages boosts preexisting tumor immunity. J Exp Med. 2018;215(3):859–76.
50. Liao D, Johnson RS. Hypoxia: a key regulator of angiogenesis in cancer. Cancer Metastasis Rev. 2007;26(2):281–90.
51. Huang H. (2018) Matrix Metalloproteinase-9 (MMP-9) as a Cancer Biomarker and MMP-9 Biosensors: Recent Advances. *Sensors (Basel)* 18(10).

Figures

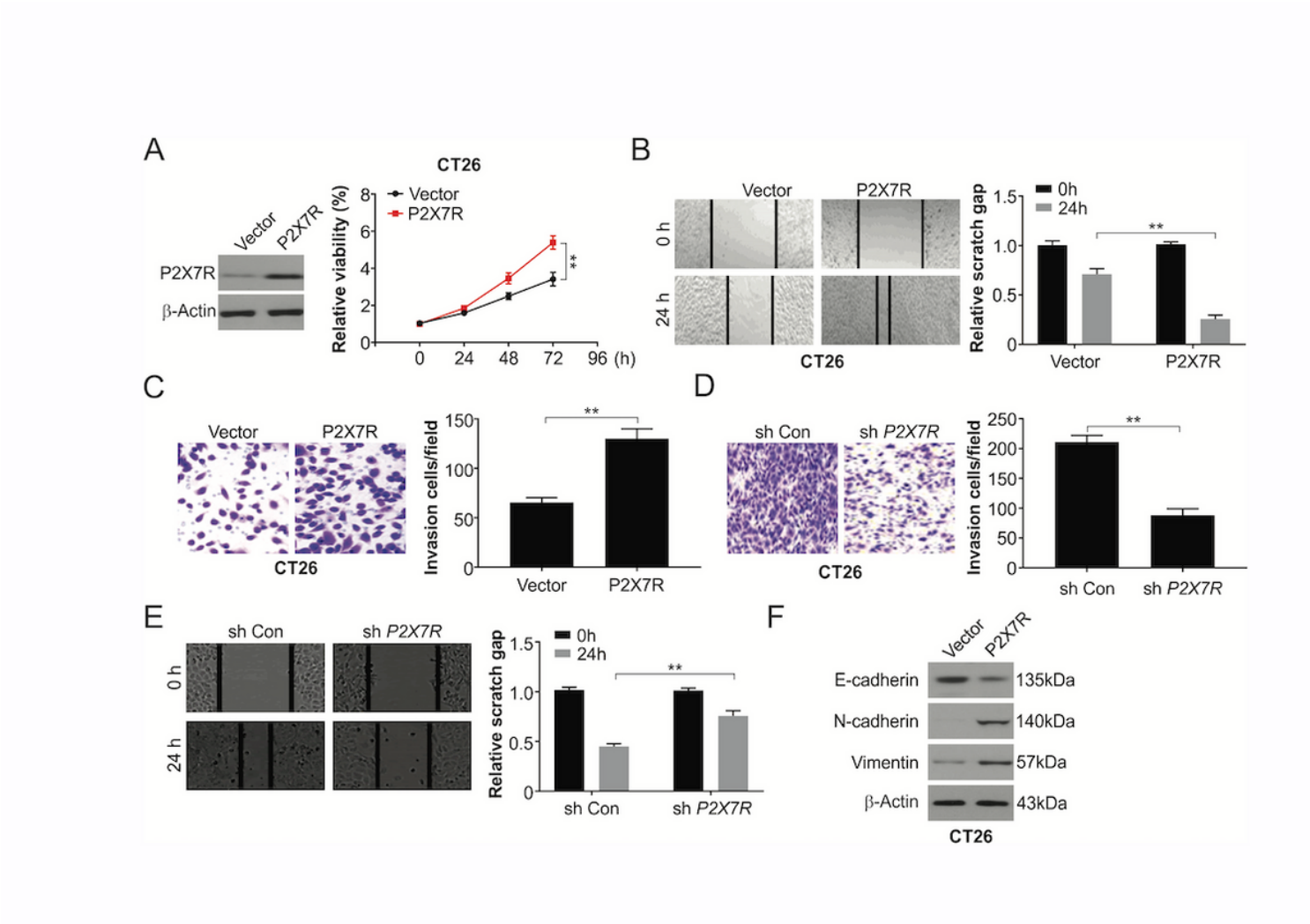

Figure 1

P2X7R promotes proliferation, migration and invasion in CRC cells. (A) Cell proliferation was determined by CCK-8 assay on the days indicated in CT26-Con and CT26-mP2X7R cells. (B) Cell migration was determined in CT26-Con and CT26-mP2X7R cells using a wound healing assay. The area of the wound was quantified to determine the extent of wound repair. (C) Cell invasion by CT26-Con and CT26-mP2X7R cells was determined using a Matrigel transwell invasion assay. The number of invading cells was quantified after crystal violet staining. (D) Cell invasion by CT26-sh Con and CT26-sh mP2X7R cells was determined using a Matrigel transwell invasion assay. The number of invading cells was quantified after crystal violet staining. (E) Cell migration by CT26-sh Con and CT26-sh mP2X7R cells was determined using a wound healing assay. The area of the wound was quantified to determine the extent of wound repair. (F) Western blotting of the indicated proteins in CT26-Con and CT26-mP2X7R cells. The results are expressed as the means ± SD of 3 independent experiments. **, P <0.01.

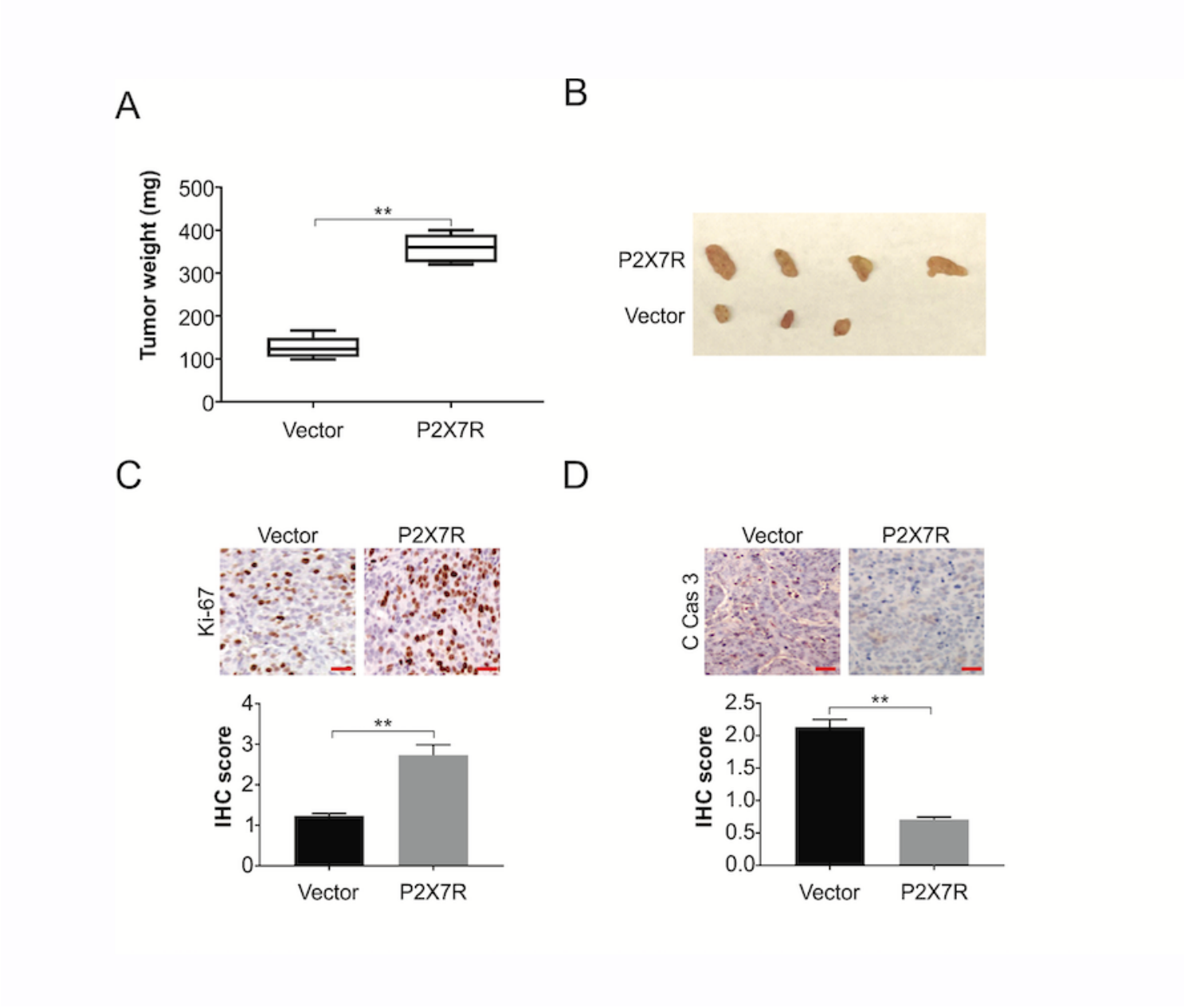

Figure 2

P2X7R overexpression increases CRC tumor growth in vivo. (A) CT26-Con or CT26-mP2X7R cells were orthotopically injected into the cecum subserosa of BALB/c mice, and the mice were killed after 6 weeks. The weight of tumors in the mice injected in the cecum with CT26-Con or isolates of CT26-mP2X7R cells. (B) Tumors from CT26-Con and CT26-mP2X7R mice. (C) The expression of Ki67 in tumors from mice injected in the cecum with CT26-Con and CT26-mP2X7R cells was analyzed by immunohistochemistry. Scale bar: 25 μm. (D) The expression of cleaved caspase-3 in tumors from mice injected in the cecum with CT26-Con and CT26-mP2X7R cells was analyzed by immunohistochemistry. Scale bar: 25 μm.

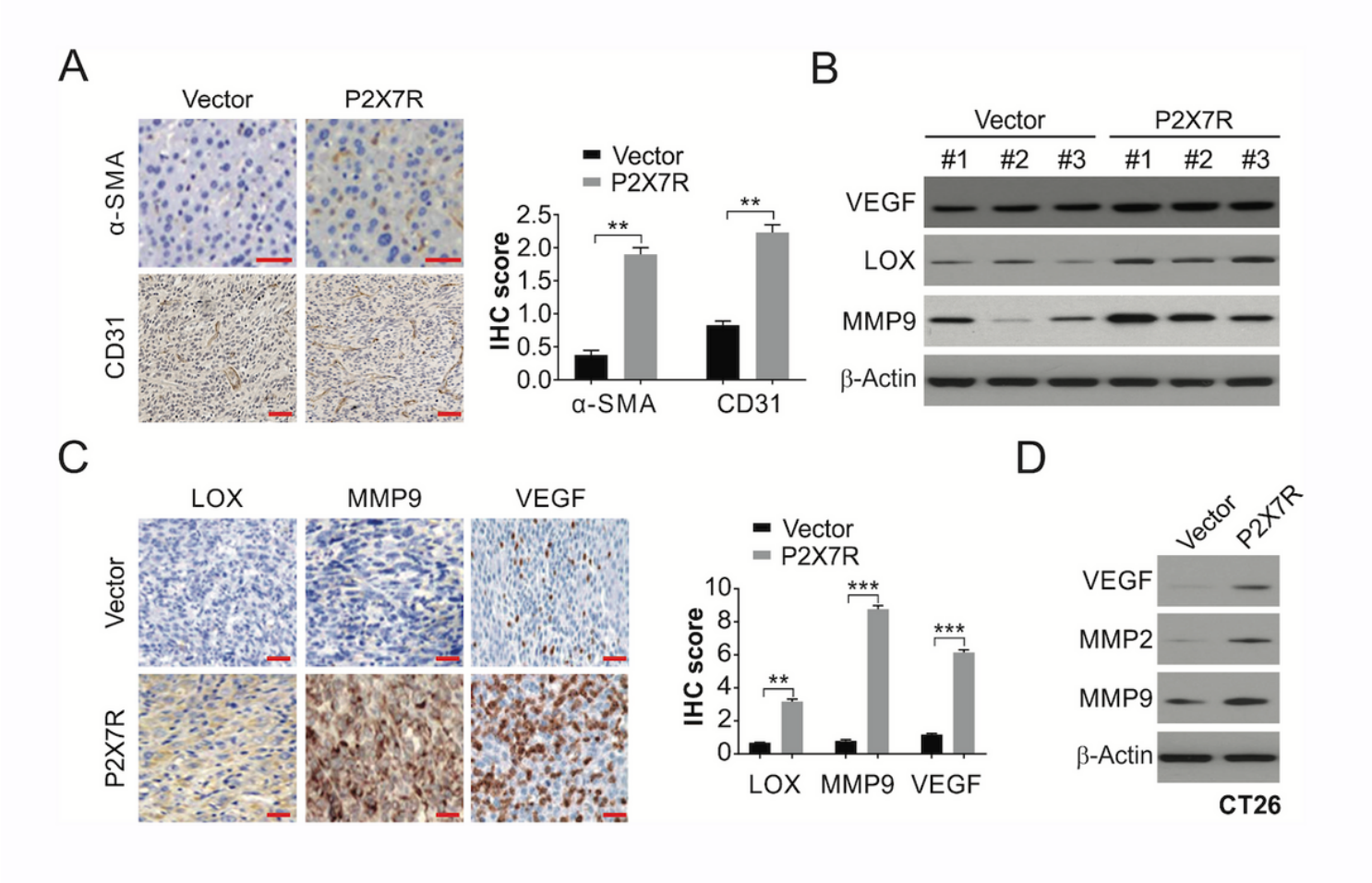

Figure 3

P2X7R overexpression promotes angiogenesis. (A) Immunohistochemical staining of CD31 and α-SMA in CT26-Con and CT26-mP2X7R tumors. Scale bar: 25 μm. (B) Western blotting of the indicated proteins in sera from CT26-mP2X7R tumor-bearing mice and CT26-Con mice. Albumin was used as a loading control. (C) The expression of MMP9, VEGF and LOX in CT26-Con and CT26-mP2X7R tumors as analyzed by immunohistochemistry. Scale bar: 25 μm. (D) Western blotting of the indicated protein in CT26-Con and CT26-mP2X7R cells.

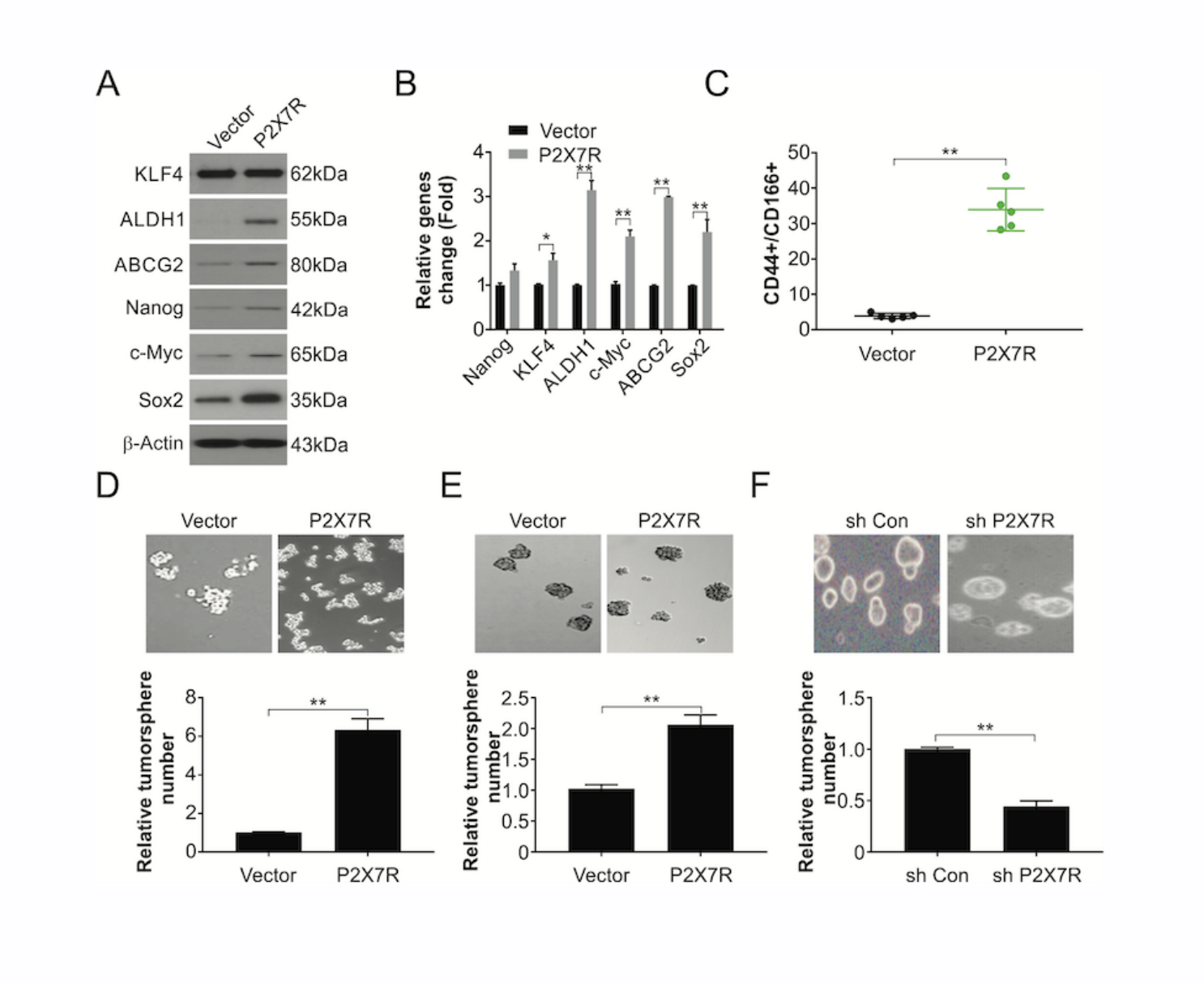

Figure 4

P2X7R overexpression in CRC cells increases CSC characteristics. (A) Western blotting of the indicated proteins in CT26-Con and CT26-mP2X7R cells. (B) mRNA levels of the indicated genes in CT26-Con and CT26-mP2X7R cells were analyzed by real-time PCR. (C) Analysis by flow cytometry of CD44 and CD166 expression in CT26-Con or CT26-mP2X7R cells. (D) Tumorspheres formation ability of CT26-Con or CT26-mP2X7R cells. (E) Tumorspheres formation ability of HCT116-Con and HCT116-P2X7R cells. (F) Tumorspheres formation ability of HCT116-sh Con and HCT116-sh P2X7R cells. The results are expressed as the means ± SD of 3 independent experiments. **, P <0.01.

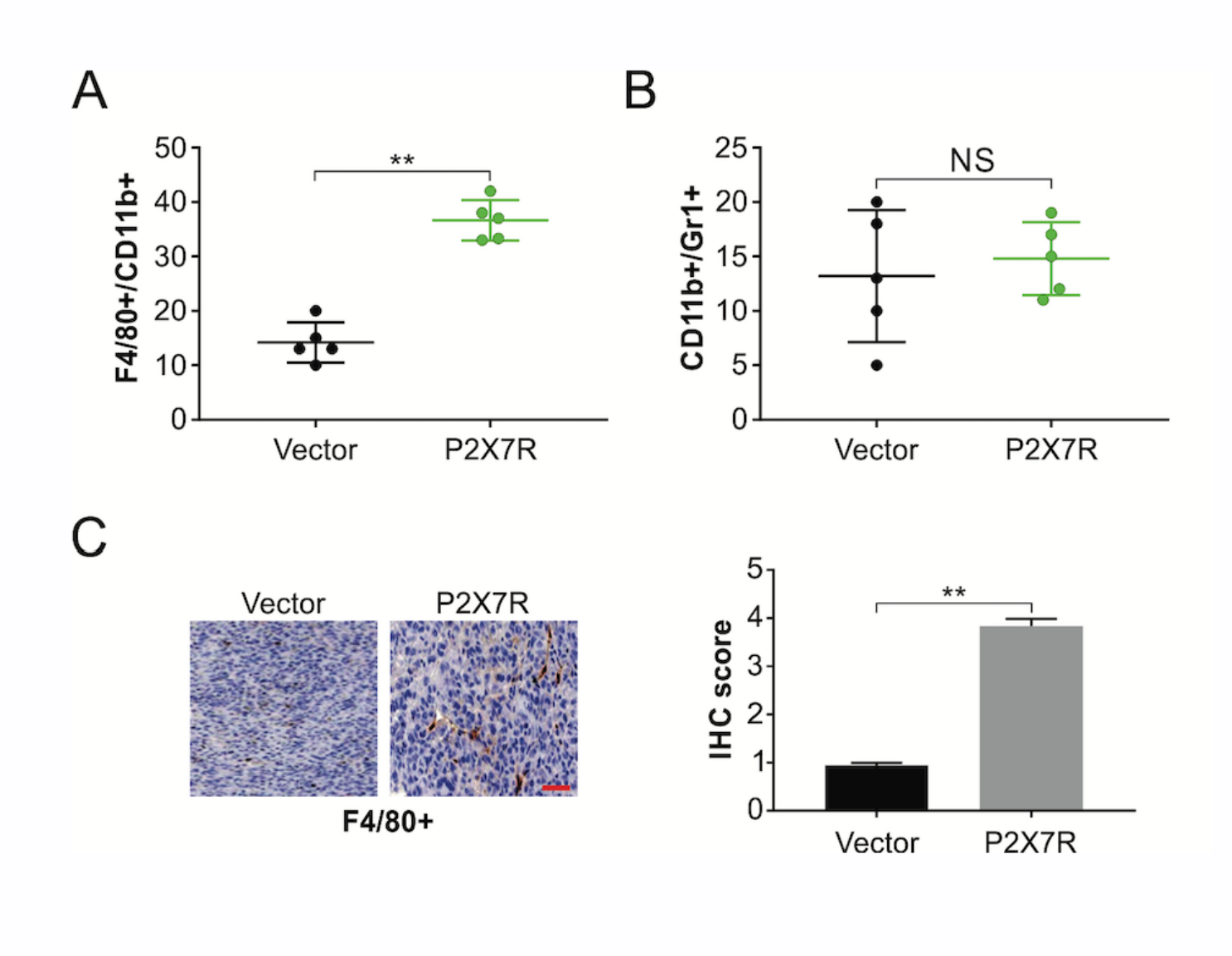

Figure 5

P2X7R promotes tumor-associated macrophage recruitment. Flow cytometry analysis of the expression of CD11b, F4/80 and Gr1 in CT26-Con and CT26-mP2X7R tumors from the cecum. (A) The percentage of total cells that were positive for either CD11b+/F4/80+ (a marker for macrophages) or (B) CD11b+/Gr1+ (a marker for neutrophils). (C) Immunohistochemical staining for the expression of F4/80 in CT26-Con- or CT26-mP2X7R-derived tumors. Scale bar: 25 μm.

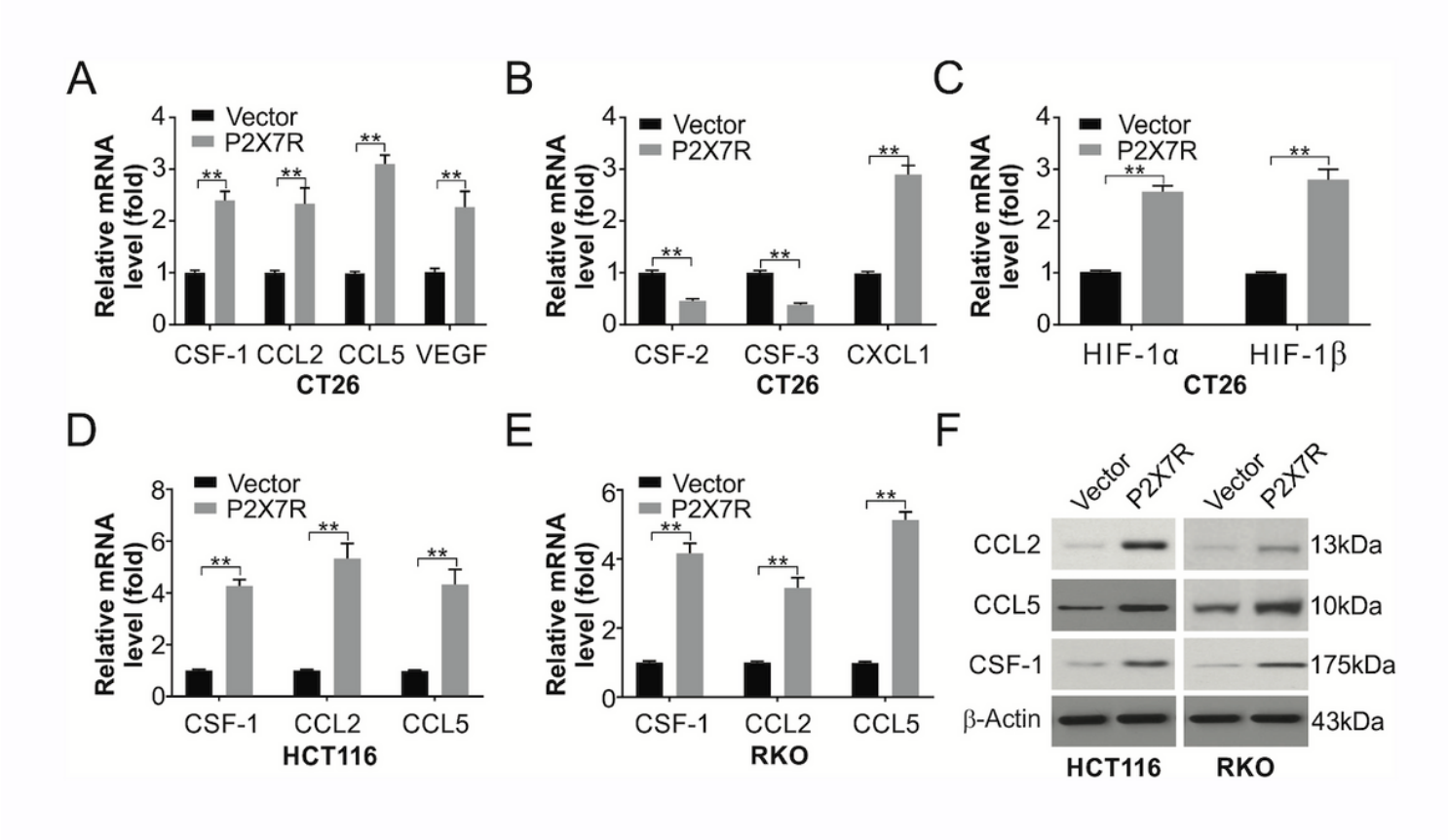

Figure 6

P2X7R overexpression in CT26 cells increases the expression of molecules that induce chemotaxis of TAMs. (A) mRNA levels of CSF-1, CCL2, CCL5 and VEGF in CT26-Con or CT26-mP2X7R cells were analyzed by real-time PCR. (B) mRNA levels of CSF-2, CSF-3 and CXCL1 in CT26-Con or CT26-mP2X7R cells were analyzed by real-time PCR. (C) mRNA levels of HIF-1α and HIF-1β in CT26-Con or CT26-mP2X7R cells were analyzed by real-time PCR. (D) mRNA levels of CCL2, CCL5 and CSF-1 in HCT116-Con or HCT116-mP2X7R cells were analyzed by real-time PCR. (E) mRNA levels of CCL2, CCL5 and CSF-1 in RKO-Con or RKO-mP2X7R cells were analyzed by real-time PCR. (F) Western blotting of CCL2, CCL5 and CSF-1 in HCT116-Con, HCT116-P2X7R, RKO-Con and RKO-P2X7R cells. The results are expressed as the means ± SD of 3 independent experiments. **, P <0.01.

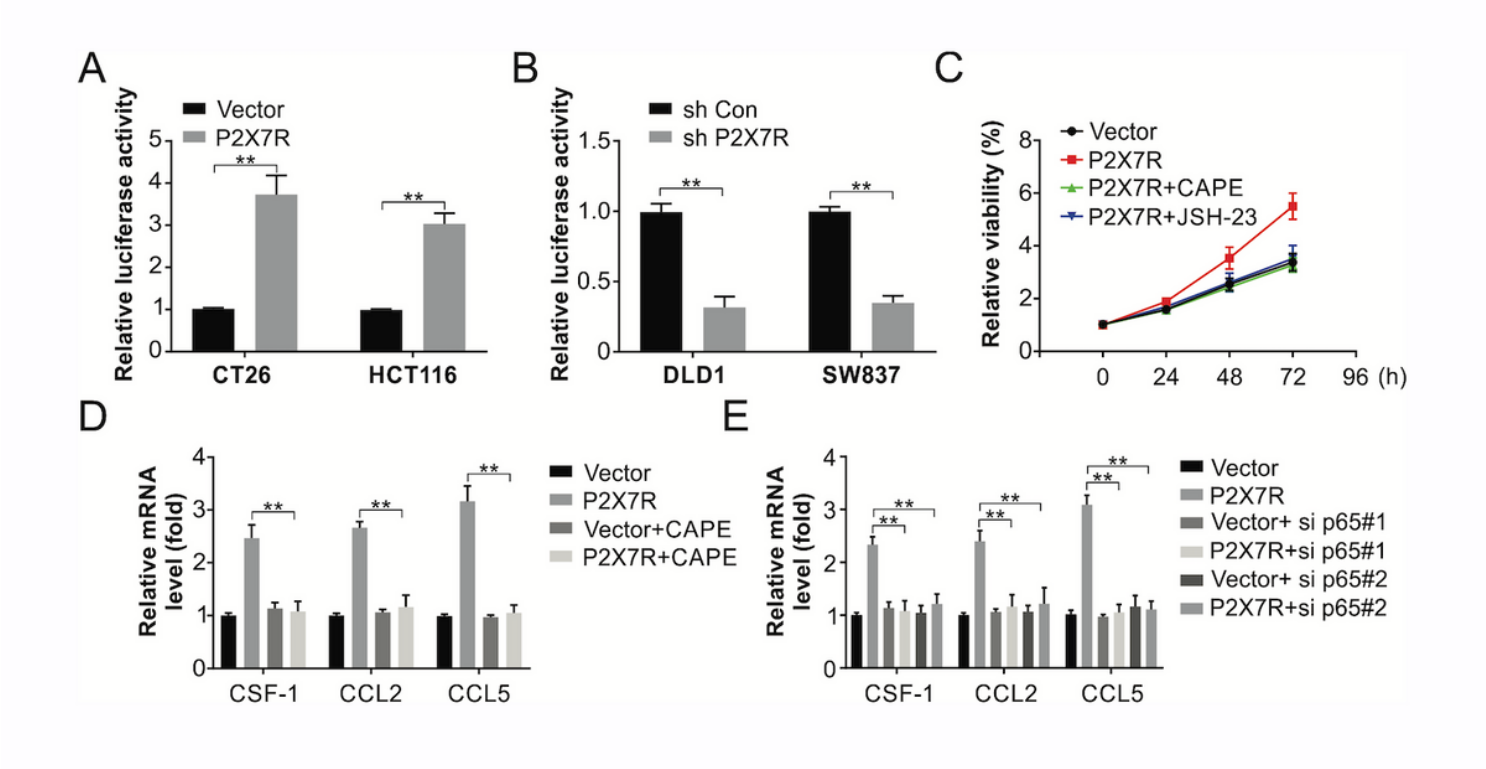

Figure 7

The NF-κB signaling pathway is responsible for P2X7R-induced cytokine expression. (A) Effects of P2X7R overexpression on the transcriptional activity of NF-κB in CT26 and HCT116 cells. (B) Effects of P2X7R knockdown on the transcriptional activity of NF-κB in DLD1 and SW837 cells. (C) Effects of CAPE and JSH-23 on cell viability of cells transfected with P2X7R. (D) Relative mRNA levels of the indicated cytokines in CT26 cells transfected with P2X7R with or without CAPE treatment. (E) Relative mRNA levels of the indicated cytokines in CT26 cells transfected with P2X7R with or without si p65 cotransfection. The results are expressed as the means ± SD of 3 independent experiments. **, P <0.01.

Supplementary Files

This is a list of supplementary files associated with this preprint. Click to download.

- Supplementaldata.docx
- Supplementaldata.docx